Genomic Regions Influencing the Hyperspectral Phenome of Deoxynivalenol Infected Wheat

Jonathan S. Concepcion
Michigan State University
Amanda D. Noble
Michigan State University
Addie M. Thompson
Michigan State University
Yanhong Dong
University of Minnesota
Eric L. Olson
eolson@msu.edu

Michigan State University

Article

Keywords:

Posted Date: February 29th, 2024

DOI: https://doi.org/10.21203/rs.3.rs-3954059/v1

Additional Declarations: No competing interests reported.

Abstract

The quantitative nature of Fusarium Head Blight (FHB) resistance requires further exploration of the wheat genome to identify regions conferring resistance. In this study, we explored the application of hyperspectral imaging of Fusarium-infected wheat kernels and identify regions of the wheat genome contributing significantly to the accumulation of Deoxynivalenol (DON) mycotoxin. Strong correlations were identified between hyperspectral reflectance values for 204 wavebands in the 397 nm to 673 nm range and DON mycotoxin. Dimensionality reduction using principal components was performed for all 204 wavebands and 38 sliding windows across the range of wavebands. PC1 of all 204 wavebands explained 70% of the total variation in waveband reflectance values and was highly correlated with DON mycotoxin. PC1 was used as a phenotype in GWAS and a large effect QTL on chromosome 2D was identified for PC1 of all wavebands as well as nearly all 38 sliding windows. The allele contributing variation in PC1 values also led to a substantial reduction in DON. The 2D polymorphism affecting DON levels localized to the exon of TraesCS2D02G524600 which is upregulated in wheat spike and rachis tissues during FHB infection. This work demonstrates the value of hyperspectral imaging as a correlated trait for investigating the genetic basis of resistance and developing wheat varieties with enhanced resistance to FHB.

Introduction

Fusarium head blight (FHB) results in significant grain quality and yield reductions that limit profits for wheat farmers and presents challenges in managing mycotoxins and affects wheat production worldwide. During FHB infection by the ascomycete fungus *Fusarium graminearum* Schwabe, Deoxynivalenol (DON) mycotoxin accumulates in wheat kernels (Mirocha et al., 1994). DON is harmful to both humans and animals when ingested (Foroud et al., 2019) and is tightly regulated by testing grain at the point of sale prior to entering the marketplace. Increasing the level of genetic resistance to FHB through breeding is a highly effective mechanism to minimize DON levels on individual farms and limit the amount of mycotoxin entering the grain marketplace (Mesterhazy 2014).

Type III resistance to FHB, resistance to DON accumulation, remains a challenge in FHB-improvement programs. As a quantitative trait, Type III resistance is controlled by multiple QTLs (Bai et al., 2018). Several QTLs for lower DON accumulation have been reported with da Silva et al. (2019) reporting a large effect QTL in 5A accounting for 13% phenotypic variation for DON. He et al. (2019) identified two major QTLs in 3B and 3D and Larkin et al. (2020) identified ten significant marker trait associations across the genome. Recently, Haile et al. (2023) identified nine QTLs associated with DON accumulation using a multi-locus GWAS model.

Phenotyping DON mycotoxin in grain samples relies on GC/MS (Gas Chromatography/Mass Spectrometry) (Tacke and Casper, 1996) methods that require extensive logistics that are time consuming and labor intensive. Obtaining samples for DON analysis requires a FHB nursery with disease pressure, extensive sampling in the field followed by threshing and milling of grain samples. High throughput

imaging technologies have been explored and exploited to improve the overall process and accuracy in phenotyping DON levels in wheat kernels (Ropelewska, 2019; Jaillais et al., 2015; Cambaza et al., 2019; Shi et al., 2020). However, DON phenotyping remains a bottleneck in elucidating the genetic basis of resistance to DON accumulation during FHB infection.

Recently, hyperspectral imaging has been explored to further increase accuracy and intensity in evaluating DON content in barley (Su et al., 2021), oats (Tekle et al., 2015; Teixido-Orries et al., 2023), and wheat (Femenias et al, 2022). At a single kernel resolution, Shen et al. (2022) and Femenias et al. (2022) imaged grain samples using wavebands at the NIR range to quantify DON. Mobile handheld hyperspectral cameras like the Specim IQ (Specim, Oulo, Finland) detect reflectance values at wavebands from the visible to near infrared (VIS/NIRS) regions (Behman et al., 2018) and have been used for disease detection of root rot in grapevine (Calamita et al., 2021), powdery mildew in wild rocket (Pane et al., 2021), and root and crown rot in sugar beet (Barreto et al., 2020).

Phenomics and imaging technologies have been integrated with genome wide association studies (GWAS) to elucidate the genetic architecture of quantitative traits (Xiao et al., 2022). Several studies have reported the integration of phenomics and high-throughput phenotyping for GWAS in wheat (Jiang et al., 2019; Rasheed et al., 2014; Yates et al., 2019), rice (Barnaby et al. 2020; Feng et al., 2017; Sun et al.,2019), soybean (Herritt et al., 2016; Dhanapal et al., 2016; Xavier et al., 2017), and maize (Muraya et al., 2017; Gage et al., 2018; Wang et al., 2019). While the genetic basis of hyperspectral imaging-derived phenotypes has been investigated in rice (Feng et al., 2017; Barnaby et al., 2020), and soybean (Wang et al., 2021; Yoosefzadeh-Najafabadi et al., 2021), great potential exists to leverage imaging technologies to investigate the genetic basis of quantitative traits.

This study leverages hyperspectral imaging in the identification of genomic regions associated with DON accumulation in soft winter wheat adapted to the Eastern United States. DON-infected wheat kernels of diverse wheat varieties and elite breeding lines were imaged using a mobile handheld hyperspectral imaging system. The hyperspectral reflectance values generated were used to 1) determine the relationship of the hyperspectral phenome with DON mycotoxin levels in wheat kernels and 2) identify genomic regions associated with mycotoxin levels and variation in the hyperspectral phenome of DON-infected kernels.

Results

Deoxynivalenol concentration

Wheat genotypes show variation for DON concentration (p-value: $3.016x10^{-7}$) based on non-parametric Kruskal-Wallis Rank Test (Fig. 1a; Supplementary Table 2). Pairwise comparison of means revealed 227 genotypes (72.3%) having significantly lower DON content in comparison with susceptible check Ambassador. In comparison 248 genotypes (79.3%) were not significantly different from the resistant check, MI14W0190 and 21 genotypes (6.7%) have significantly lower DON content than MI14W0190.

Hyperspectral reflectance values and dimensionality reduction of the hyperspectral phenome

Significant variation among the genotypes based on Kruskal-Wallis Rank Test and ANOVA F-Test for wavebands meeting normality and variance homogeneity assumptions, were observed in each of the 204 wavebands generated (Supplementary Table 2; Supplementary Fig. 1). Of the 204 wavebands evaluated, only 15 wavebands (7.35%) met the normality and variance homogeneity assumptions (Supplementary Table 2). Significant positive correlations were found between the 204 wavebands generated and DON content, with 97 wavebands in the 455 nm to 739 nm range demonstrating a correlation of greater than 0.5 with DON content (Supplementary Table 3). The 584 nm to 673 nm waveband range demonstrated the highest correlations with DON greater than 0.6 (Supplementary Table 3).

Principal component analysis was performed for all 204 wavebands and the first two principal components accounted for 74.0% and 6.0% of variation in hyperspectral reflectance values (Supplementary Table 6), respectively. Genotypes having lower PC1 values demonstrated lower DON content and PC1 of all wavebands was correlated with DON at 0.57. The waveband at 502 nm demonstrated the highest component loading (0.101) and was also found to be the most discriminatory among the wavebands, followed by 499 nm, 505 nm, 508 nm, and 511 nm (Supplementary Table 4). Wavebands in the 397 nm to 780 nm demonstrated higher component loading than most wavebands beyond 780 nm (Supplementary Table 4).

Principal component analysis was also carried out for binned wavebands using a sliding window approach. The first principal component for each of the 38 binned wavebands (windows) explained 51–99% of the variation in hyperspectral reflectance values within each bin (Supplementary Table 6). PC1 of each waveband bin was found to be significantly correlated with DON content (Fig. 2, Supplementary Table 7). Windows 1 to 10 spanning wavebands 397 nm to 584 nm demonstrated significant positive correlations of 0.50 to 0.58 with GC/MS-derived DON content, while Windows 11 to 25 spanning wavebands 542 nm to 810 nm demonstrated a significant negative correlation from − 0.40 to -0.64 (Fig. 2; Supplementary Table 7). The sign of the correlation between waveband window PC1 values and DON inverted six times across the waveband spectrum (Fig. 2). The correlation of PC1 with DON inverted from positive in Window 1 to 10 to negative from Windows 11 to 25. Correlation with DON inverted again from Windows 25 to 26, 27 to 28, 29 to 30 and 33 to 34.

Genome wide association study for deoxynivalenol accumulation

GWAS was performed to identify marker trait associations (MTAs) associated with DON content (Supplementary Table 8). Five significant MTAs were identified in chromosomes 2A, 2B, 3A, and 5A explaining 1.96–4.03% of the variation in DON (Table 1, Supplementary Table 8, Supplementary File 1). Favorable alleles at all five loci demonstrated a reduction in DON content (Fig. 3)

Table 1
Marker-trait associations identified using GC/MS-derived DON content as phenotypic input influencing DON accumulation.

Significant SNP (MTA)	Chromosome	Position (mb)	Allele*	p.value	Alleles Effect	PVE (%)
S2A_PART2_18053	2A	642.9	**A**/G	**6.11×10^{-8}**	3.77	3.85
S2B_PART2_24719	2B	700.4	**T**/C	**6.68×10^{-7}**	2.47	1.39
S3A_PART2_25234	3A	706.4	**C**/T	**6.32×10^{-7}**	3.64	2.65
S3A_PART2_25425	3A	708.4	**C**/T	**9.82×10^{-7}**	4.24	4.03
S5A_PART1_18813	5A	18.81	**C**/T	**4.65×10^{-7}**	2.88	1.96
*Alleles in bold reduce DON accumulation						
PVE = Phenotypic Variance Explained						

GWAS using PC1 of all 204 wavebands identifies a single locus on chromosome 2D (S2D_PART2_15090) at 613.12 Mb on chromosome 2D was identified using PC1 explaining 26.4% of the phenotypic variation in the hyperspectral phenome of DON-infected wheat kernels (Fig. 3). Genotypes carrying the A allele demonstrate a 6.3 ppm reduction in DON compared with genotypes bearing the G allele (Fig. 4c, Supplementary Table 8). The A allele at the 2D locus is the minor allele with a high frequency of 0.47.

GWAS using the PC1 value for all 38 waveband bins consistently identifies the 2D locus in 35 of the 38 waveband bins, explaining 6.4–28.3% of the phenotypic variation in PC1. The S2D_PART2_15090 SNP demonstrates a negative allele effect from Windows 1 to 10 (397 nm to 584 nm) and a positive allele effect from Windows 11 to 25 (543 nm to 811 nm). The inversion of allele effect is consistent with the observed change in sign in the correlation between waveband bin PC1 values and DON content.

An additional 18 MTAs were identified across the hyperspectral phenome of DON infected wheat kernels on chromosomes 1A, 1B, 1D, 2B, 2D, 3A, 3B, 4A, 4B, 7A, 7B and 7D (Supplementary Table 8, Supplementary File 1) across different waveband ranges. A locus on 1B was identified from 396 nm to 467 nm explaining 18.8% and 17.6% of variation in PC1 of waveband reflectance values and reducing DON by 2.0 ppm and 2.2 ppm at waveband bins 1 and 2, respectively (Supplementary Table 8). Other MTAs explained 0.2–7.6% of variation in PC1 of reflectance values within individual waveband bins.

Several SNPs significantly associated with waveband bin PC1 values were found to be in LD (Supplementary Table 9). On chromosome 2D, the SNPs S2D_PART2_13700 and S2D_PART2_15090, were found to be in high LD with r2 = 0.88 at substantial distance of 13.9 mb (Supplementary Table 9).

Weaker LD was detected between SNPs S2B_PART2_28124 and S2B_PART2_27654 on chromosome 2B at a distance of 4.69 mb (r^2 = 0.72), and between SNPs S1B_PART2_24837 and S1B_PART2_24652 on chromosome 1B (distance: 1.85 mb) (r^2 = 0.25).

Putative candidate gene identified on chromosome 2D

The SNP identified on 2D associated with PC1 of the entire hyperspectral phenome of DON infected wheat kernels and PC1 of nearly all sliding windows, S2D_PART2_15090, is located in the single exon of a 1,104 kb gene, *TraesCS2D02G524600*, coding for a protein with an F-box domain. *TraesCS2D02G524600* is upregulated in the spikelets and rachis in response to inoculation with *F. graminearum* in near-isogenic lines (NILs) bearing a 2DL introgression conferring FHB resistance (Biselli et al. 2018) (Supplementary Fig. 5) and has been implicated in *Fhb1* resistance with higher expression in NILs carrying *Fhb1* (Ma et al., 2021) (Supplementary Fig. 6). The expression of *TraesCS2D02G524600* and 17 adjacent genes within a 2Mb region, 1Mb upstream and downstream, was investigated across tissues and developmental stages under *F. graminearum* infection (Wheat Expression Browser, Ramirez-Gonzalez et al., 2021) (Supplementary Fig. 7). *TraesCS2D02G524600* is inducible by infection with *F. graminearum* and highly expressed in the spike at the reproductive stage, which is consistent across gene expression data sets. Only one gene in the 2Mb interval, *TraesCS2D02G524400*, located upstream of *TraesCS2D02G524600*, demonstrates the exact same expression profile. TraesCS2D02G524600 is a likely candidate gene for the large effect locus on 2D that reduces DON accumulation in wheat kernels during infection by *F. graminearum*.

Discussion

Breeding for resistance to FHB requires evaluation of the multiple components of resistance (Steiner et al., 2017). Each FHB resistance component has a different relationship to DON (Buerstmayr and Lemmens, 2015, Mesterhazy et al., 2015, Paul et al., 2005) and evaluating multiple traits can lead to better selection decisions in breeding. Visual observations of FHB severity and incidence are used to develop an overall visual FHB index (Steiner et al., 2017). The proportion of Fusarium damaged kernels can be estimated on samples of infected grain and a high correlation with DON has been demonstrated for this resistance component (Mesterhazy et al., 2015).

In this study, we generate multiple visual FHB resistance phenotypes using the hyperspectral phenome of DON infected wheat kernels. Reflectance values at individual wavebands can be considered unique phenotypes and high correlations were found between DON and reflectance values at individual wavebands, especially at the visible light spectrum range. PC1 of the reflectance values from all wavebands compresses the entire hyperspectral phenome into a single phenotype that incorporates the information from all wavebands. The hyperspectral phenome was dissected further into 38 sliding windows and PC1 of each window was used as a separate phenotype that is correlated with DON.

In this study, we identified five MTAs on chromosomes 2A, 2B, 3A, and 5A that co-localize with previously reported genomic regions conferring resistance to DON (Supplementary Table 10). Individually, each of

the MTAs identified for DON content explain only 1–4% of the variation in DON and reduce DON by 2.5 ppm to 4.2 ppm. FHB resistance traits can differ in their genetic architecture. Developing the hyperspectral phenome into a novel FHB resistance phenotype using PC1 of all wavebands, which is correlated to DON, led to identification of a comparably large effect locus on 2D explaining 26% of the variation in PC1 and reducing DON by 6.8 ppm. While several genomic regions were identified across waveband ranges, the 2D locus was identified using PC1 across waveband ranges, further establishing its association with the hyperspectral phenome of DON infected whet kernels. By leveraging the hyperspectral phenome as a correlated trait, we were able to identify a locus influencing the target trait, DON mycotoxin content.

The large effect locus on 2D localizes to the exon of an F-box protein encoding gene and captures a large proportion of variation in the hyperspectral phenome of DON infected wheat kernels. Two SNPs were identified in the exon of this gene; however, the BLINK algorithm removes SNPs that are in LD. Multiple gene expression studies demonstrate the gene is inducible upon infection with *F. graminearum* and is expressed exclusively in tissues of the spike and rachis as a component of the defense response. It may be possible to select for the DON-reducing allele at 2D locus in a breeding context using a Kompetitive Allele Specific PCR (KASP) marker assay (He et al., 2014).

Evaluation of DON production during infection by *F. graminearum* is an integral part in developing wheat varieties with resistance to Fusarium Head Blight (FHB), which has long been done using GC/MS (Tacke and Casper, 1996). Preparation and phenotyping of DON infected wheat kernel samples is time consuming, tedious, and labor intensive (Steiner et al., 2017). This study demonstrates that hyperspectral imaging can reduce the amount of time and physical resources necessary to make selection decisions in breeding for lower DON.

Methods

Plant materials

A set of 200 soft red and 114 soft white winter wheat genotypes (n = 314), comprised of advanced breeding lines and commercial varieties (Supplementary Table 1) were used in this study. Genotypes MI14W0190 and Ambassador were considered checks FHB-resistant, low DON and FHB-susceptible, high DON checks, respectively. Wheat genotypes were planted in a misted and inoculated Fusarium screening nursery in East Lasing, MI (º42.69 N, º84.48W, Elevation: 264 m) in one-meter rows using a completely randomized designed with two to four replicates per genotype.

Fusarium inoculum

Fusarium graminearum cultures were collected in 2020 from Huron, Ingham, Monroe, Tuscola and Sanilac counties in Michigan, USA. Initial cultures were grown by placing infected seed in Nash-Synder Media for 5 to 7 days at room temperature. Isolates for field inoculation were cultured in spawn bags with 0.2-micron filter patch (Unicorn Bags, TX, USA) containing 1.5 kg corn kernels. Corn was soaked in

deionized (DI) water for 24 to 48 hours and autoclaved three times for 90 minutes. One culture plate of a four to six days-old culture and 100 ml autoclaved deionized water were added to each spawn bag. Cultures developed over two to three weeks and were dried in biohazard hood for 48 hours at ambient temperature. Isolates from different locations were cultured separately. After drying, *F. graminearum* grain spawn cultures from the five locations were pooled in equal proportions by weight prior to inoculation. Field inoculation was carried out five times beginning at approximately 5 weeks prior to flowering. A misting system was run throughout the nursery 10 minutes every hour for 12 hours, 6 am to 6 pm, to promote infection and disease development.

Deoxynivalenol evaluation

Wheat heads from the middle 0.3 meter of each row were sampled separately and harvested by hand. The heads from each row were threshed together and all seeds were retained. A subsample of 10 grams from each row was ball-milled using Restch MM 400 miller (Retsch, PA, USA) to generate flour meeting the guidelines set by the US Wheat and Barley Scab Initiative (USWBI) (https://scabusa.org/don_labs_umn_testinglab_protocol). Deoxynivalenol concentration of flour samples was determined using Gas Chromatography / Mass Spectrometry (GC/MS) at the Department of Plant Pathology, University of Minnesota.

Hyperspectral image acquisition

FHB-infected wheat kernels from each genotype sent for DON content measurement were imaged using, a handheld, push broom hyperspectral camera, Specim IQ (Specim, Oulo, Finland). A sample of 50 to 80 wheat kernels from each replicate of each genotype were imaged. Seeds were placed against a black background side-by-side with the white reference panel. Imaging was done inside a 51 x 51 x 51-centimeter light box (Finnhomy, USA) using the attached LED light source. The hyperspectral camera was mounted on a tripod and angled 45º facing downward over the kernels. Default Recording Mode was used to capture reflectance values from 204 wavebands from 397 to 1004 nm with an integration time of 30 to 40 seconds and focus set at automatic.

Image processing and reflectance value extraction

Hyperspectral images were processed using QGIS 3.10.2 (QGIS, 2020). Image files (.dat) were imported as raster layer. Rendering was carried out using multiband color with Band 088 (651.92 nm) as Red Band, Band 057 (560.30 nm) as Green Band, and Band 037 (501.72) as Blue Band. Color enhancements were set at Stretch to MinMax and normal blending mode. Raster calculation was carried out at 0.3 to 0.8 threshold. Raster calculated images were saved as GeoTIFF (.tif) file and converted to vector image (Polygonize) using default settings. To determine region of interest (wheat kernels) and remove unnecessary features, toggle editing by selecting features was used. Vectorized images with region of interest determined were saved as ESRI Shape File (.shp). Spectral reflectance values were extracted from each ESRI shape file using “raster” package (Hijmans et al., 2023) in R v4.2.2 (R Core Team, 2021) by calculating mean reflectance values in each waveband.

Statistical analysis

The normality of hyperspectral reflectance data was assessed using Shapiro-Wilk Test and variance homogeneity assumption was carried out using Levene's Test. Wavebands with p-values < 0.05 failed to meet normality and homogeneity assumption. To test variation among the wheat genotypes for DON content and spectral reflectance values in all 204 wavebands, ANOVA was carried out for reflectance values at wavebands meeting normality and homogeneity assumptions, otherwise non-parametric Kruskal-Wallis Rank Test was employed following the model:

$$y = G + e$$

Where y is the DON content or spectral reflectance value of each waveband, G is the fixed effect of genotype, and e is the residual. Shapiro-Wilk Test, Levene's Test, ANOVA F-Test, and Kruska-Wallis Rank Test were carried out in R v4.2.2 (R Core Team, 2021).

Means of DON content and spectral reflectance values for two to four replicates per genotype were calculated using the "emmeans" package (Lenth et al., 2018). Pearson's Correlation Coefficient was computed between DON means and spectral reflectance values at all individual wavebands.

Principal Component Analysis of wavebands

Principal Component Analysis was carried out using reflectance values for all wavebands to dimensionally reduce the spectral data and identify wavebands potentially associated with DON. To evaluate the contribution of waveband ranges across the hyperspectral phenome of DON infected wheat kernels, we employed a "Sliding Window" approach where the first twenty wavebands were binned and subjected to Principal Component Analysis. The bin was then "slid" at five-waveband intervals and PCs were generated for the next twenty wavebands to 1004 nm for a total of 38 windows (binned wavebands). The resulting PC1 waveband reflectance values from the 38 windows were then correlated to the GC/MS-derived DON content and used as predictors of DON. PCA and correlation was carried out in R v4.2.2 (R Core Team, 2021).

DNA isolation and genotyping

Tissue was collected from all genotypes evaluated and DNA was isolated according to Wiersma et al. (2016). Genotyping-by-sequencing libraries were prepared according to Poland et al. (2012) scaled to a 24uL volume in 384-well format. Libraries were sequenced at 384-plex on an Illumina HiSeq 4000 instrument. Single nucleotide polymorphisms (SNPs) were called using the TASSEL 5 GBS pipeline (Glaubitz et al., 2014). Reads were aligned to the RefSeq v1.0 wheat reference genome assembly (International Wheat Genome Sequencing Consortium) using default parameters. For the GBSSeqToTagDBPlugin and ProductionSNPCallerPluginV2 steps, the k-mer length was set to 64 base pairs and a minimum coverage of five reads was required for each k-mer. Default settings were used for all other steps. SNPs were initially called using all families and parents. SNPs were subsequently filtered for 0.85 call rate and 0.05 MAF.

Genome wide association mapping

Phenotypes for Genome Wide Association (GWAS) included: 1) GC/MS-derived DON content, 2) PC1 of all 204 wavebands and 3) PC1 of 38 waveband bins from the “Sliding Window” approach. GWAS was carried out using the Bayesian-information and Linkage Disequilibrium Iteratively Nested Keyway (BLINK) (Huang et al., 2019) model in GAPIT v3 (Genomic Association and Prediction Integrated Tool) (Lipka et al., 2012; latest version: March 12, 2022). A total of 9,961 SNPs across all 21 chromosomes remained after filtering at minor allele frequency (MAF) < 0.05 and 0.85 call rate. To address potential population structure, three principal components were used in GWAS models with the exception of two principal components for one phenotypic input, and four principal components for four phenotypic inputs (Supplementary Table 7). Linkage disequilibrium between Marker-Trait Associations (MTAs) was investigated using TASSEL 5 (Glaubitz et al., 2014).

Candidate gene identification

Significant SNPs identified in GWAS were assigned to high confidence gene models in IWGSC RefSeq Annotation V1.0 (www.wheatgenome.org). Descriptions of putative candidate genes were derived from the public wheat expression database Triticeae Multi-omics center (http://202.194.139.32) (Ma et al., 2021) and Wheat Expression Browser (Ramirez-Gonzalez et al., 2021).

Declarations

Author Contribution

EO and JC conceptualized the study, AN designed and established FHB nursery, YD analyzed DON concentration, JC acquired hyperspectral images, AT supported the hyperspectral image processing, JC processed and analyzed hyperspectral images, JC and EO conducted statistical analyses, JC wrote the first draft of the manuscript, EO wrote portions and revised the manuscript. All authors have read and contributed to the manuscript. The authors declare no conflict of interest.

Data Availability

All data used in this study, including the raw and processed hyperspectral images, phenotypic (DON) data, and genotypic data are available as per request.

Acknowledgements

The authors would like to acknowledge Amelia Orr, Samantha Mitchell, Dennis Pennington, Elizabeth Ross, Sadie Finegan, Maddie Pennington, and Jordan Parish for their assistance in field establishment and maintenance, and sample harvesting and preparation. The authors would also like to acknowledge Dr. Katherine Frels (University of Nebraska), Dr. Francisco Gomez (Syngenta) and Dr. Leonardo Volpato (Corteva) for their insights. This project was supported by AFRI Competitive Grant 2022-68013-36439 (WheatCAP) from the USDA-NIFA, The US Wheat and Barley Scab Initiative under USDA-ARS agreement 59-0206-2-135 and The Michigan Wheat Program agreement: 15-08-03-ES.

References

1. Mirocha, C. J. *et al.* Production of trichothecene mycotoxins by *Fusarium graminearum* and *Fusarium culmorum* on barley and wheat. Mycopathologia 128, 19–23 (1994).
2. Foroud, N. A. *et al.* Trichothecenes in Cereal Grains – An Update. Toxins 11, 634 (2019).
3. Mesterházy, Á. Breeding for Resistance to Fusarium Head Blight in Wheat. in *Mycotoxin Reduction in Grain Chains* 189–208 (John Wiley & Sons, Ltd, 2014). doi:10.1002/9781118832790.ch13.
4. Bai, G., Su, Z. & Cai, J. Wheat resistance to Fusarium head blight. Canadian Journal of Plant Pathology 40, 336–346 (2018).
5. da Silva, C. *et al.* QTL mapping of Fusarium head blight resistance and deoxynivalenol accumulation in the Kansas wheat variety 'Everest'. Mol Breeding 39, 35 (2019).
6. He, X., Dreisigacker, S., Singh, R. P. & Singh, P. K. Genetics for low correlation between Fusarium head blight disease and deoxynivalenol (DON) content in a bread wheat mapping population. Theor Appl Genet 132, 2401–2411 (2019).
7. Larkin, D. L. *et al.* Genome-wide analysis and prediction of Fusarium head blight resistance in soft red winter wheat. Crop Science 60, 2882–2900 (2020).
8. Haile, J. K. *et al.* Multi-locus genome-wide association studies reveal the genetic architecture of Fusarium head blight resistance in durum wheat. Front. Plant Sci. 14, 1182548 (2023).
9. Tacke, B. K. & Casper, H. H. Determination of deoxynivalenol in wheat, barley, and malt by column cleanup and gas chromatography with electron capture detection. J AOAC Int 79, 472–475 (1996).
10. Ropelewska, E. Post-harvest assessment of wheat and barley kernel infections with fungi of the genus Fusarium using thermal analysis. Journal of Stored Products Research 83, 61–65 (2019).
11. Jaillais, B., Roumet, P., Pinson-Gadais, L. & Bertrand, D. Detection of Fusarium head blight contamination in wheat kernels by multivariate imaging. Food Control 54, 250–258 (2015).
12. Cambaza, E., Koseki, S. & Kawamura, S. Why RGB Imaging Should be Used to Analyze Fusarium Graminearum Growth and Estimate Deoxynivalenol Contamination. *MPs* 2, 25 (2019).
13. Shi, Y., Liu, W., Zhao, P., Liu, C. & Zheng, L. Rapid and nondestructive determination of deoxynivalenol (DON) content in wheat using multispectral imaging (MSI) technology with chemometric methods. Anal. Methods 12, 3390–3396 (2020).
14. Su, W.-H. *et al.* Hyperspectral imaging and improved feature variable selection for automated determination of deoxynivalenol in various genetic lines of barley kernels for resistance screening. Food Chemistry 343, 128507 (2021).
15. Tekle, S., Måge, I., Segtnan, V. H. & Bjørnstad, Å. Near-Infrared Hyperspectral Imaging of *Fusarium* -Damaged Oats (Avena *sativa* L.). Cereal Chem 92, 73–80 (2015).
16. Teixido-Orries, I., Molino, F., Femenias, A., Ramos, A. J. & Marín, S. Quantification and classification of deoxynivalenol-contaminated oat samples by near-infrared hyperspectral imaging. Food Chemistry 417, 135924 (2023).

17. Femenias, A., Llorens-Serentill, E., Ramos, A. J., Sanchis, V. & Marín, S. Near-infrared hyperspectral imaging evaluation of Fusarium damage and DON in single wheat kernels. Food Control 142, 109239 (2022).
18. Shen, G. *et al.* Rapid and nondestructive quantification of deoxynivalenol in individual wheat kernels using near-infrared hyperspectral imaging and chemometrics. Food Control 131, 108420 (2022).
19. Calamita, F., Imran, H. A., Vescovo, L., Mekhalfi, M. L. & La Porta, N. Early Identification of Root Rot Disease by Using Hyperspectral Reflectance: The Case of Pathosystem Grapevine/Armillaria. Remote Sensing 13, 2436 (2021).
20. Pane, C., Manganiello, G., Nicastro, N., Cardi, T. & Carotenuto, F. Powdery Mildew Caused by Erysiphe cruciferarum on Wild Rocket (Diplotaxis tenuifolia): Hyperspectral Imaging and Machine Learning Modeling for Non-Destructive Disease Detection. Agriculture 11, 337 (2021).
21. Barreto, A., Paulus, S., Varrelmann, M. & Mahlein, A.-K. Hyperspectral imaging of symptoms induced by Rhizoctonia solani in sugar beet: comparison of input data and different machine learning algorithms. J Plant Dis Prot 127, 441–451 (2020).
22. Behmann, J. *et al.* Specim IQ: Evaluation of a New, Miniaturized Handheld Hyperspectral Camera and Its Application for Plant Phenotyping and Disease Detection. Sensors 18, 441 (2018).
23. Xiao, Q., Bai, X., Zhang, C. & He, Y. Advanced high-throughput plant phenotyping techniques for genome-wide association studies: A review. Journal of Advanced Research 35, 215–230 (2022).
24. Jiang, L. *et al.* Functional mapping of N deficiency-induced response in wheat yield-component traits by implementing high-throughput phenotyping. The Plant Journal 97, 1105–1119 (2019).
25. Rasheed, A. *et al.* Genome-wide association for grain morphology in synthetic hexaploid wheats using digital imaging analysis. BMC Plant Biol 14, 128 (2014).
26. Yates, S. *et al.* Precision Phenotyping Reveals Novel Loci for Quantitative Resistance to Septoria Tritici Blotch. Plant Phenomics 2019, 2019/3285904 (2019).
27. Barnaby, J. Y. *et al.* Vis/NIR hyperspectral imaging distinguishes sub-population, production environment, and physicochemical grain properties in rice. Sci Rep 10, 9284 (2020).
28. Feng, H. *et al.* An integrated hyperspectral imaging and genome-wide association analysis platform provides spectral and genetic insights into the natural variation in rice. Sci Rep 7, 4401 (2017).
29. Sun, D. *et al.* Using hyperspectral analysis as a potential high throughput phenotyping tool in GWAS for protein content of rice quality. Plant Methods 15, 54 (2019).
30. Herritt, M., Dhanapal, A. P. & Fritschi, F. B. Identification of Genomic Loci Associated with the Photochemical Reflectance Index by Genome-Wide Association Study in Soybean. The Plant Genome 9, plantgenome2015.08.0072 (2016).
31. Dhanapal, A. P. *et al.* Genome-wide association mapping of soybean chlorophyll traits based on canopy spectral reflectance and leaf extracts. BMC Plant Biol 16, 174 (2016).
32. Xavier, A., Hall, B., Hearst, A. A., Cherkauer, K. A. & Rainey, K. M. Genetic Architecture of Phenomic-Enabled Canopy Coverage in *Glycine max*. Genetics 206, 1081–1089 (2017).

33. Muraya, M. M. *et al.* Genetic variation of growth dynamics in maize (Zea *mays* L.) revealed through automated non-invasive phenotyping. The Plant Journal 89, 366–380 (2017).
34. Gage, J. L., De Leon, N. & Clayton, M. K. Comparing Genome-Wide Association Study Results from Different Measurements of an Underlying Phenotype. *G3 Genes|Genomes|Genetics* 8, 3715–3722 (2018).
35. Wang, L. *et al.* Identification of the QTL-allele System Underlying Two High-Throughput Physiological Traits in the Chinese Soybean Germplasm Population. Frontiers in Genetics 12, (2021).
36. Wang, X. *et al.* Dynamic plant height QTL revealed in maize through remote sensing phenotyping using a high-throughput unmanned aerial vehicle (UAV). Sci Rep 9, 3458 (2019).
37. Yoosefzadeh-Najafabadi, M., Torabi, S., Tulpan, D., Rajcan, I. & Eskandari, M. Genome-Wide Association Studies of Soybean Yield-Related Hyperspectral Reflectance Bands Using Machine Learning-Mediated Data Integration Methods. Frontiers in Plant Science 12, (2021).
38. Biselli, C. *et al.* Comparative Transcriptome Profiles of Near-Isogenic Hexaploid Wheat Lines Differing for Effective Alleles at the 2DL FHB Resistance QTL. Front. Plant Sci. 9, 37 (2018).
39. Ma, S. *et al.* WheatOmics: A platform combining multiple omics data to accelerate functional genomics studies in wheat. Mol Plant 14, 1965–1968 (2021).
40. Ramírez-González, R. H. *et al.* The transcriptional landscape of polyploid wheat. Science 361, eaar6089 (2018).
41. Steiner, B. *et al.* Breeding strategies and advances in line selection for Fusarium head blight resistance in wheat. Trop. plant pathol. 42, 165–174 (2017).
42. Buerstmayr, H. & Lemmens, M. Breeding healthy cereals: genetic improvement of Fusarium resistance and consequences for mycotoxins. World Mycotoxin Journal 8, 591–602 (2015).
43. Mesterházy, A. *et al.* Breeding for FHB Resistance via Fusarium Damaged Kernels and Deoxynivalenol Accumulation as Well as Inoculation Methods in Winter Wheat. Agricultural Sciences 06, 970 (2015).
44. Paul, P. A., Lipps, P. E. & Madden, L. V. Relationship Between Visual Estimates of Fusarium Head Blight Intensity and Deoxynivalenol Accumulation in Harvested Wheat Grain: A Meta-Analysis. *Phytopathology®* 95, 1225–1236 (2005).
45. He, C., Holme, J. & Anthony, J. SNP Genotyping: The KASP Assay. in Crop Breeding (eds. Fleury, D. & Whitford, R.) vol. 1145 75–86 (Springer New York, New York, NY, 2014).
46. Hijmans, R. J. *et al.* raster: Geographic Data Analysis and Modeling. (2023).
47. R Development Core Team. R: A language and environment for statistical computing. (2021).
48. Lenth, R. V. *et al.* emmeans: Estimated Marginal Means, aka Least-Squares Means. (2024).
49. Wiersma, A. T. *et al.* Fine mapping of the stem rust resistance gene SrTA10187. Theor Appl Genet 129, 2369–2378 (2016).
50. Poland, J. A., Brown, P. J., Sorrells, M. E. & Jannink, J.-L. Development of High-Density Genetic Maps for Barley and Wheat Using a Novel Two-Enzyme Genotyping-by-Sequencing Approach. PLOS ONE 7,

e32253 (2012).

51. Glaubitz, J. C. *et al.* TASSEL-GBS: A High Capacity Genotyping by Sequencing Analysis Pipeline. PLoS ONE 9, e90346 (2014).
52. Huang, M., Liu, X., Zhou, Y., Summers, R. M. & Zhang, Z. BLINK: a package for the next level of genome-wide association studies with both individuals and markers in the millions. *GigaScience* 8, (2019).
53. Lipka, A. E. *et al.* GAPIT: genome association and prediction integrated tool. Bioinformatics 28, 2397–2399 (2012).
54. Buerstmayr, M. & Buerstmayr, H. Comparative mapping of quantitative trait loci for Fusarium head blight resistance and anther retention in the winter wheat population Capo × Arina. Theor Appl Genet 128, 1519–1530 (2015).
55. Buerstmayr, M., Alimari, A., Steiner, B. & Buerstmayr, H. Genetic mapping of QTL for resistance to Fusarium head blight spread (type 2 resistance) in a Triticum dicoccoides × Triticum durum backcross-derived population. Theor Appl Genet 126, 2825–2834 (2013).
56. Buerstmayr, M. *et al.* Mapping of QTL for Fusarium head blight resistance and morphological and developmental traits in three backcross populations derived from Triticum dicoccum × Triticum durum. Theor Appl Genet 125, 1751–1765 (2012).
57. Bonin, C. M. & Kolb, F. L. Resistance to Fusarium Head Blight and Kernel Damage in a Winter Wheat Recombinant Inbred Line Population. Crop Science 49, 1304–1312 (2009).
58. Dhariwal, R. *et al.* High Density Single Nucleotide Polymorphism (SNP) Mapping and Quantitative Trait Loci (QTL) Analysis in a Biparental Spring Triticale Population Localized Major and Minor Effect Fusarium Head Blight Resistance and Associated Traits QTL. Genes 9, 19 (2018).
59. Eckard, J. T., Glover, K. D., Mergoum, M., Anderson, J. A. & Gonzalez-Hernandez, J. L. Multiple Fusarium head blight resistance loci mapped and pyramided onto elite spring wheat Fhb1 backgrounds using an IBD-based linkage approach. Euphytica 204, 63–79 (2015).
60. Garvin, D. F., Stack, R. W. & Hansen, J. M. Quantitative Trait Locus Mapping of Increased Fusarium Head Blight Susceptibility Associated with a Wild Emmer Wheat Chromosome. *Phytopathology®* 99, 447–452 (2009).
61. Gervais, L. *et al.* Mapping of quantitative trait loci for field resistance to Fusarium head blight in an European winter wheat. Theor Appl Genet 106, 961–970 (2003).
62. Herter, C. P. *et al.* Rht24 reduces height in the winter wheat population 'Solitär × Bussard' without adverse effects on Fusarium head blight infection. Theor Appl Genet 131, 1263–1272 (2018).
63. Jiang, G.-L., Dong, Y., Shi, J. & Ward, R. W. QTL analysis of resistance to Fusarium head blight in the novel wheat germplasm CJ 9306. II. Resistance to deoxynivalenol accumulation and grain yield loss. Theor Appl Genet 115, 1043–1052 (2007).
64. Lin, F. *et al.* Mapping QTL associated with resistance to Fusarium head blight in the Nanda2419 × Wangshuibai population. I. Type II resistance. Theor Appl Genet 109, 1504–1511 (2004).

65. Lu, Q. *et al.* Two Major Resistance Quantitative Trait Loci are Required to Counteract the Increased Susceptibility to Fusarium Head Blight of the Rht-D1b Dwarfing Gene in Wheat. Crop Science 51, 2430–2438 (2011).
66. Lu, Q. *et al.* Anther extrusion and plant height are associated with Type I resistance to Fusarium head blight in bread wheat line 'Shanghai-3/Catbird'. Theor Appl Genet 126, 317–334 (2013).
67. Ma, H.-X., Bai, G.-H., Zhang, X. & Lu, W.-Z. Main Effects, Epistasis, and Environmental Interactions of Quantitative Trait Loci for Fusarium Head Blight Resistance in a Recombinant Inbred Population. *Phytopathology®* 96, 534–541 (2006).
68. Mardi, M. *et al.* QTL analysis of resistance to Fusarium head blight in wheat using a 'Wangshuibai'-derived population. Plant Breeding 124, 329–333 (2005).
69. McCartney, C. A. *et al.* Fusarium Head Blight Resistance QTL in the Spring Wheat Cross Kenyon/86ISMN 2137. Frontiers in Microbiology 7, (2016).
70. Miedaner, T., Kalih, R., Großmann, M. S. & Maurer, H. P. Correlation between Fusarium head blight severity and DON content in triticale as revealed by phenotypic and molecular data. Plant Breeding 135, 31–37 (2016).
71. Miedaner, T. *et al.* Broad-spectrum resistance loci for three quantitatively inherited diseases in two winter wheat populations. Mol Breeding 29, 731–742 (2012).
72. Otto, C. D., Kianian, S. F., Elias, E. M., Stack, R. W. & Joppa, L. R. Genetic dissection of a major Fusarium head blight QTL in tetraploid wheat. Plant Mol Biol 48, 625–632 (2002).
73. Paillard, S. *et al.* QTL analysis of resistance to Fusarium head blight in Swiss winter wheat (Triticum aestivum L.). Theor Appl Genet 109, 323–332 (2004).
74. Petersen, S. *et al.* Mapping of Fusarium Head Blight Resistance Quantitative Trait Loci in Winter Wheat Cultivar NC-Neuse. Crop Science 56, 1473–1483 (2016).
75. Petersen, S. *et al.* Validation of Fusarium Head Blight Resistance QTL in US Winter Wheat. Crop Science 57, 1–12 (2017).
76. Ren, J. *et al.* Detection and validation of a novel major QTL for resistance to Fusarium head blight from Triticum aestivum in the terminal region of chromosome 7DL. Theor Appl Genet 132, 241–255 (2019).
77. Szavo-Herver, A. *et al.* Differential influence of QTL linked to Fusarium head blight, Fusarium-damaged kernel, deoxynivalenol contents and associated morphological traits in a Frontana-derived wheat population. Euphytica 200, 9–26 (2014).
78. Ruan, Y. *et al.* Identification of novel QTL for resistance to Fusarium head blight in a tetraploid wheat population. Genome 55, 853–864 (2012).
79. Sari, E. *et al.* High density genetic mapping of Fusarium head blight resistance QTL in tetraploid wheat. PLoS ONE 13, e0204362 (2018).
80. Shah, L. *et al.* Quantitative trait loci associated to Fusarium head blight resistance in wheat populations containing Annong–1124 and Zhoumai–27. Physiological and Molecular Plant

Pathology 100, 67–74 (2017).

81. Srinivasachary, S. *et al.* Mapping of QTL associated with Fusarium head blight in spring wheat RL4137. Czech J. Genet. Plant Breed. 44, 147–159 (2008).
82. Tacke, B. K. & Casper, H. H. Determination of deoxynivalenol in wheat, barley, and malt by column cleanup and gas chromatography with electron capture detection. J AOAC Int 79, 472–475 (1996).
83. He, X., Dreisigacker, S., Singh, R. P. & Singh, P. K. Genetics for low correlation between Fusarium head blight disease and deoxynivalenol (DON) content in a bread wheat mapping population. Theor Appl Genet 132, 2401–2411 (2019).
84. Zhang, Q. *et al.* Identification and molecular mapping of quantitative trait loci for Fusarium head blight resistance in emmer and durum wheat using a single nucleotide polymorphism-based linkage map. Mol Breeding 34, 1677–1687 (2014).
85. Zhang, W. *et al.* Genetic characterization of type II Fusarium head blight resistance derived from transgressive segregation in a cross between Eastern and Western Canadian spring wheat. Mol Breeding 38, 13 (2018).
86. Zhang, G. & Mergoum, M. Molecular mapping of kernel shattering and its association with Fusarium head blight resistance in a Sumai3 derived population. Theor Appl Genet 115, 757–766 (2007).
87. Zhou, W. *et al.* Molecular characterization of Fusarium head blight resistance in Wangshuibai with simple sequence repeat and amplified fragment length polymorphism markers. Genome 47, 1137–1143 (2004).
88. Zhu, X. *et al.* Toward a better understanding of the genomic region harboring Fusarium head blight resistance QTL Qfhs.ndsu-3AS in durum wheat. Theor Appl Genet 129, 31–43 (2016).

Figures

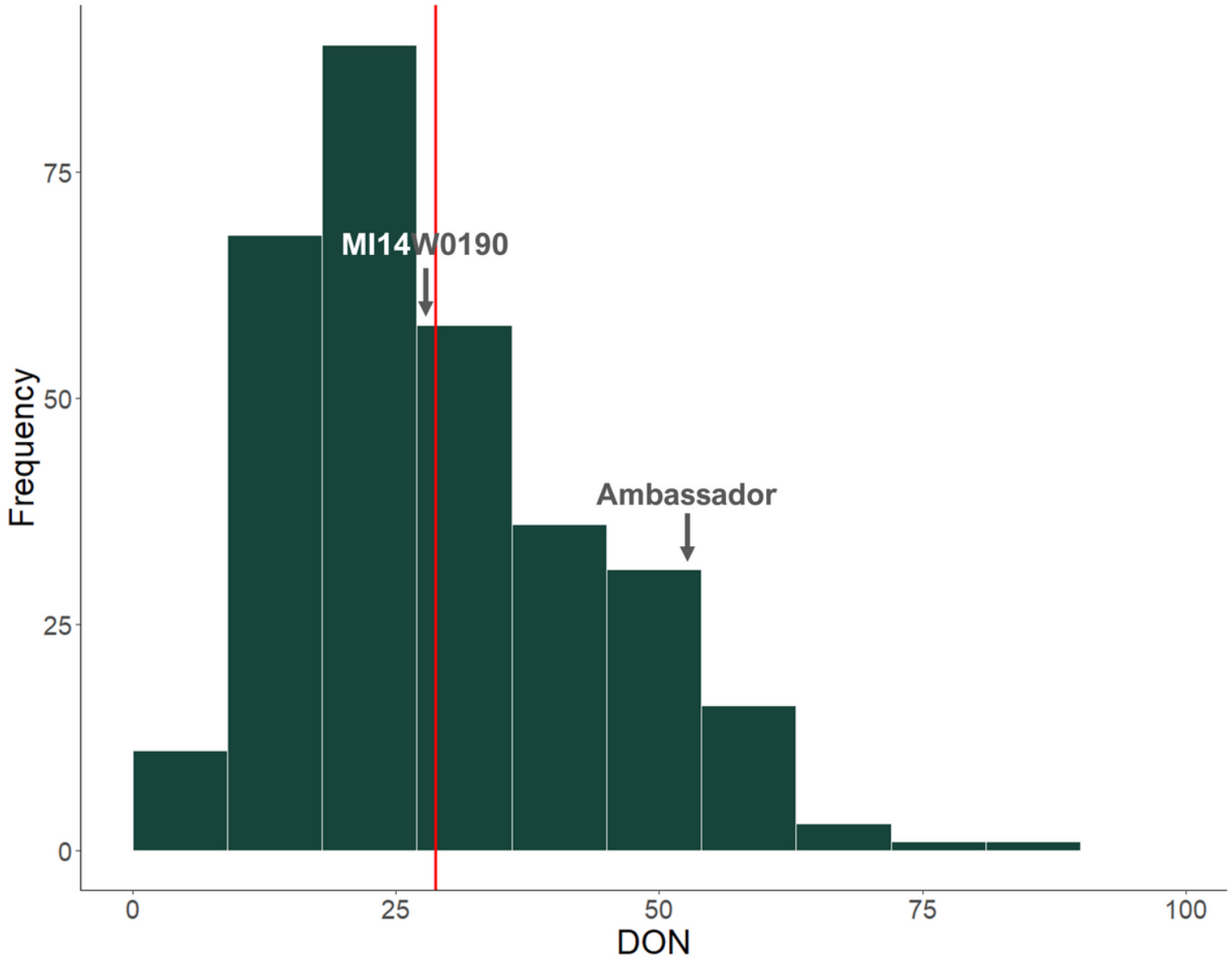

Figure 1

Phenotyping of soft winter wheat genotypes for DON accumulation. Frequency distribution of GC/MS-derived DON content of the 314 soft winter wheat genotypes (red line represents the population mean DON content).

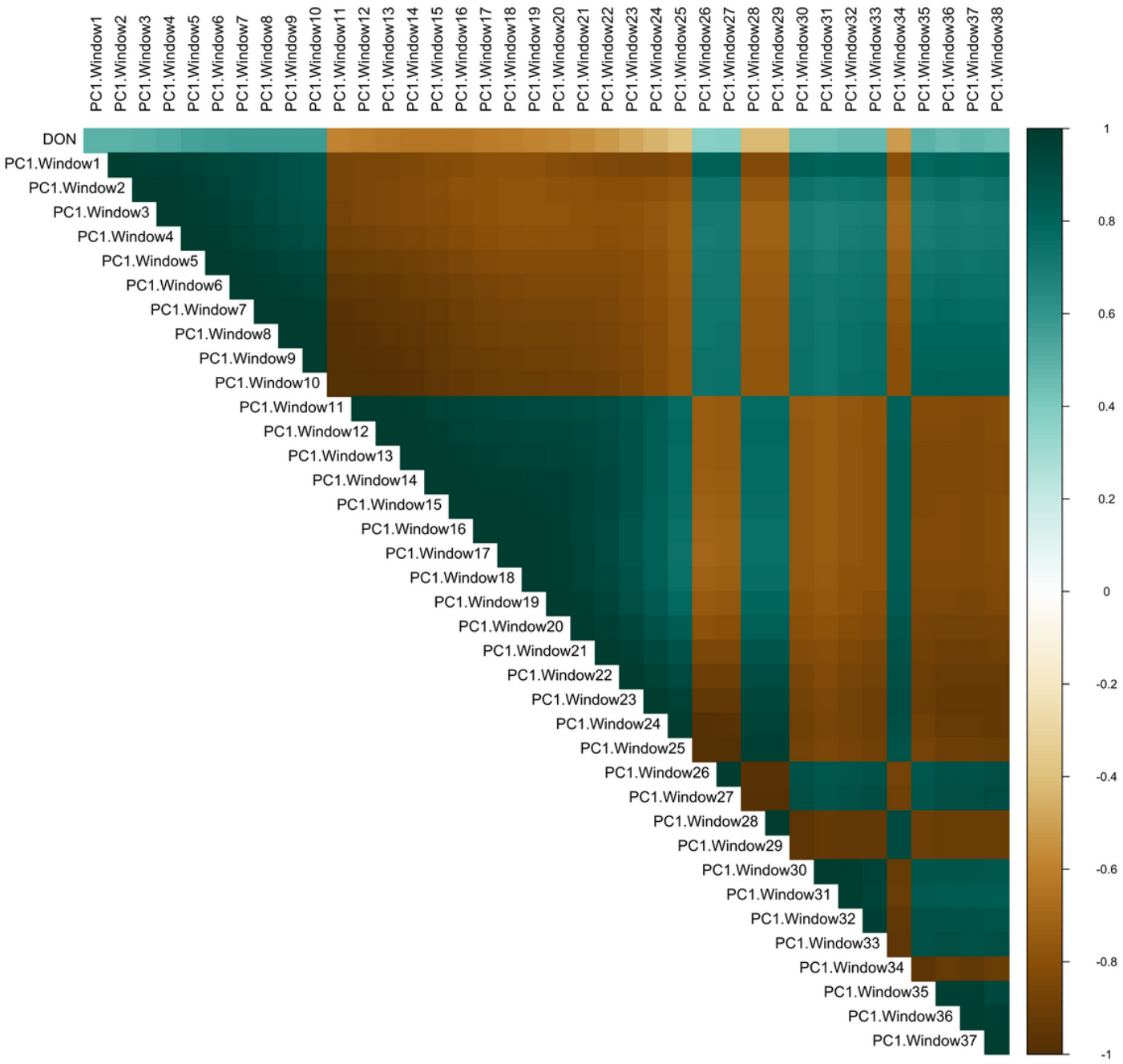

Figure 2

Heatmap of correlations among PC1 between 38 sliding windows (binned wavebands) and DON content.

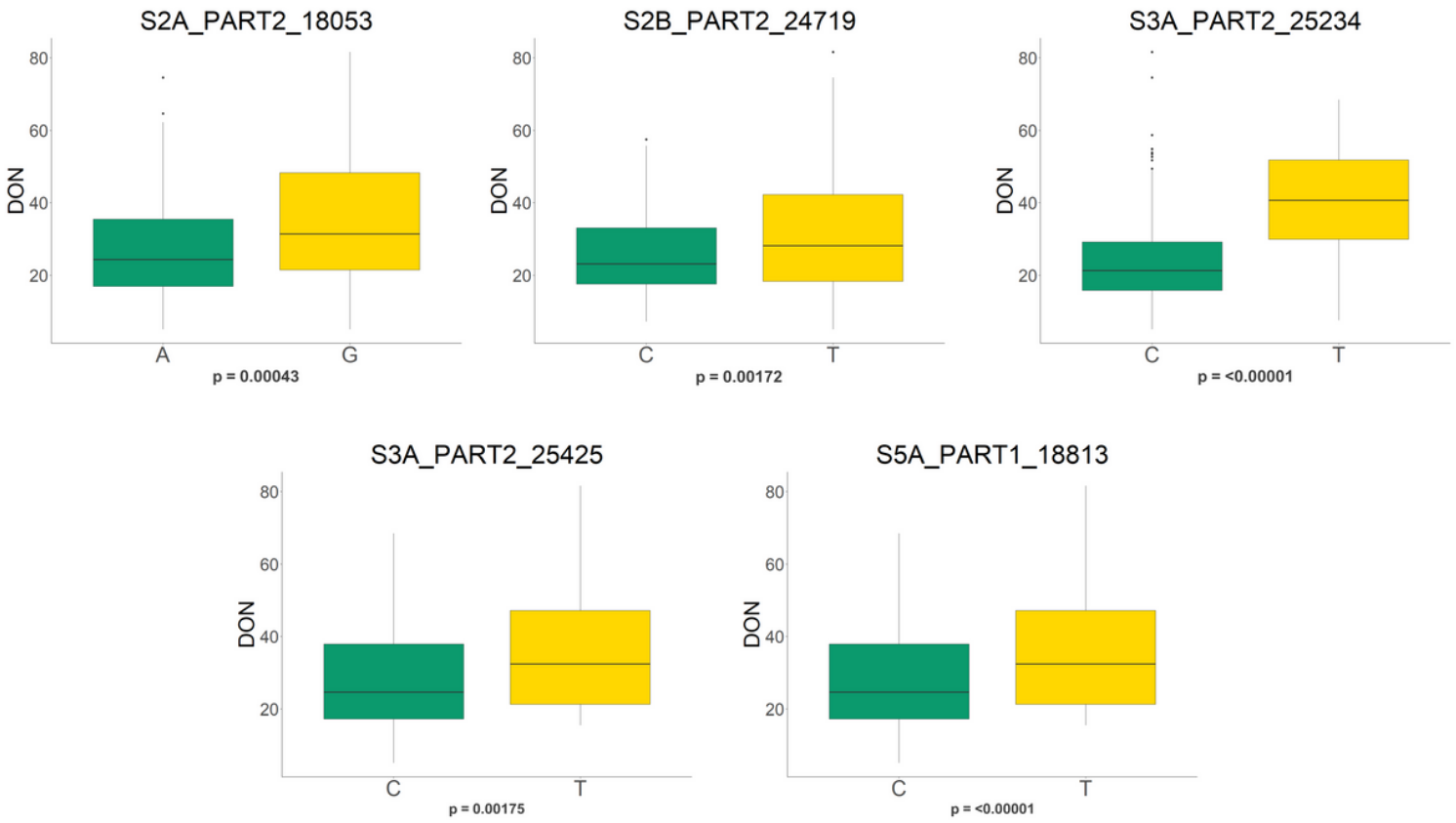

Figure 3

Alleles reducing GC/MS-derived DON identified by GWAS.

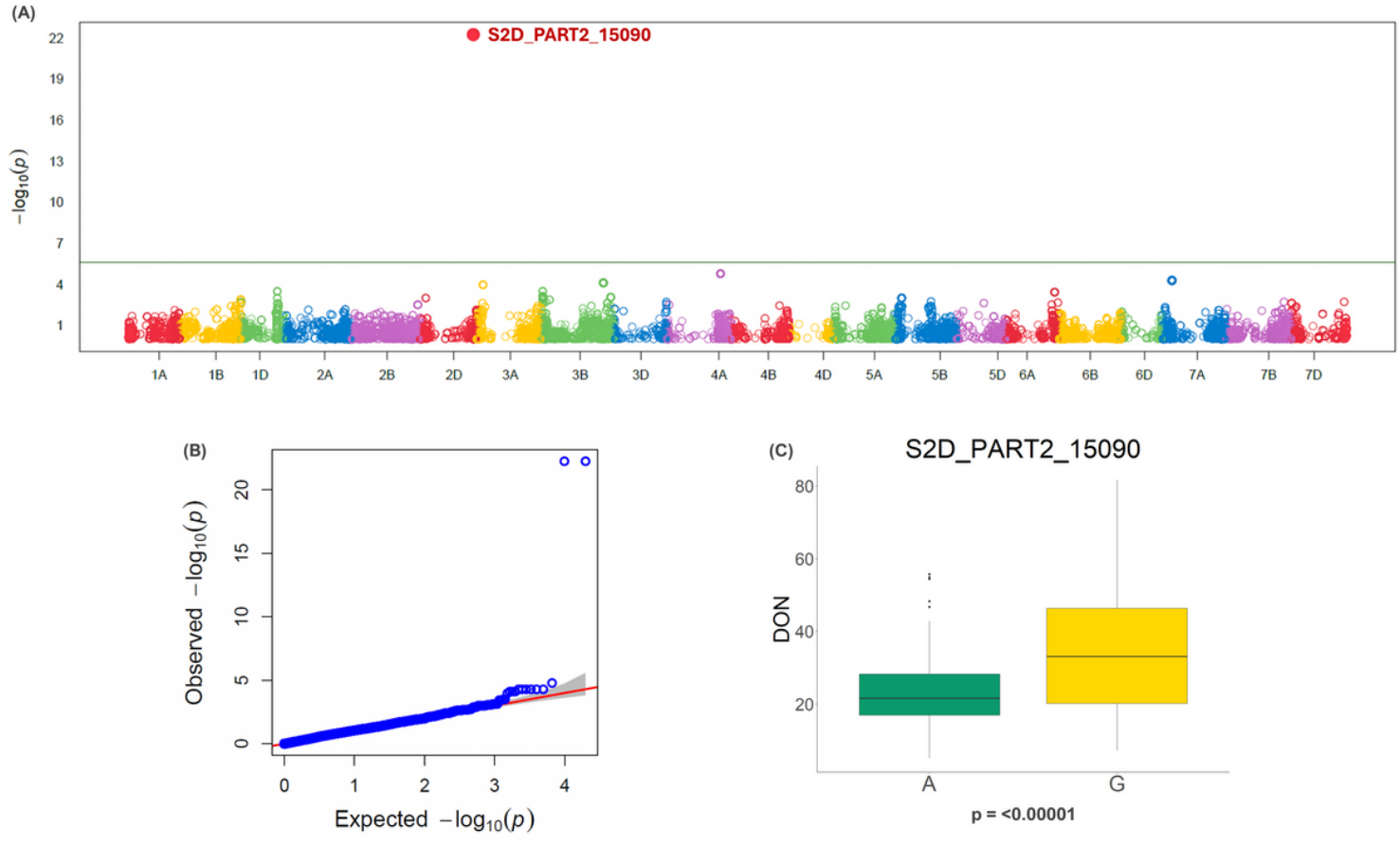

Figure 4

Genome wide association using PC1 of the 204 wavebands generated using hyperspectral imaging. (a) Manhattan plot identifying the MTA on chromosome 2DL and (b) its corresponding quantile-quantile plot, (c) variation in actual DON content of genotypes carrying the A and G allele in SNP S2D_PART2_15090.

Supplementary Files

This is a list of supplementary files associated with this preprint. Click to download.

- SupplementaryFigures.docx
- SupplementaryFile1.docx
- SupplementaryFile2.docx
- SupplementaryTables.xlsx